From Intra- to Intermolecular Hydrogen Bond with the Surrounding: Steady-State and Time-Resolved Behaviours

Noemí Alarcos,[1≠] Mario Gutierrez,[1≠] Marta Liras,[2] Félix Sánchez,[2] and Abderrazzak Douhal[1*]

[1]Departamento de Química Física, Facultad de Ciencias Ambientales y Bioquímica, and INAMOL, Universidad de Castilla-La Mancha, Avenida Carlos III, S.N., 45071 Toledo, Spain.

[2] Instituto de Química Orgánica General, IQOG-CSIC, Juan de la Cierva, 3, 28006 Madrid, Spain

≠ Equal contributions

*Corresponding author at Universidad de Castilla-La Mancha.

Tel.: +34 925 265717; E-mail address: abderrazzak.douhal@uclm.es

Abstract

We report on the photodynamics of 2-(2'-hydroxyphenyl)benzoxazole (HBO), compared to its amino derivatives 6-amino-2-(2'-hydroxypheny)benzoxazole (6A-HBO) and 5-amino-2-(2'-hydroxypheny)benzoxazole (5A-HBO) in N, N-dimethylformamide (DMF) solutions. HBO at S_0 shows a reversible deprotonation reaction leading to the production of anion forms. While for 6A-HBO and 5A-HBO, DMF containing KOH is necessary to get the anions. Excited HBO in DMF exhibits intra- as well as intermolecular proton transfer (ESIPT and ESPT) reactions. Exciting at 330 nm, we observed the open-enol, anti-enol and keto forms with different emission and lifetimes (620 ps, 1.5 ns, 74 ps, respectively). While exciting at 433 nm, only the anion species emission was detected (3.7 ns). Contrary to HBO, 6A-HBO and 5A-HBO do not exhibit any proton transfer process, and only the emission of the open-enol charge-transferred forms (open-ECT) was observed, which is comparable to those of their methylated derivatives (6A-MBO and 5A-MBO). Femtosecond studies of 6A-MBO and 6A-HBO in DMF indicate that an intramolecular charge-transfer (ICT) reaction (~80 fs) and solvent relaxation processes (2 ps) take place at S_1. Remarkably, the photoinduced breaking of the intramolecular hydrogen bond for 6A-HBO and formation of the intermolecular one with DMF molecules occur in 80 ps, while for 5A-HBO, this happen in less of 10 ps. In this work, we demonstrate that the presence and position of the amino group in the HBO framework change both S_0 and S_1 behaviours of the intramolecular H-bonds, a result which might be useful for the design and better understanding of supramolecular systems based on intra- and intermolecular H-bonds.

Keywords: solvent relaxation, benzoxazole, photodynamics, proton and charge transfer, H-bond.

1.   Introduction

The hydroxyphenylbenzazole's family has been studied during the last three decades because of their ability to undergo ultrafast (femtosecond regime) excited-state intramolecular proton transfer (ESIPT) reactions to form phototautomers.[1-16] Among these molecules, 2-(2'-hydroxyphenyl)benzoxazole (HBO),[1, 8, 9, 13, 15-18] 2-(2'-hydroxyphenyl)benzothiazole (HBT)[2, 5, 12, 19-24] and 2-(2'-hydroxyphenyl)benzimidazole (HBI),[3, 4, 25] show changes in their photobehavior with the solvent. In aprotic and/or nonpolar media, the ESIPT reaction takes place,[1, 4, 8, 15, 17, 23-26] while in polar protic solvents it has to compete with excited-state intermolecular proton transfer (ESPT) one due to the H-bonding formed between the dye and the solvent molecules.[2, 9, 12, 13, 15, 17, 18, 21, 27] For example, HBO in polar aprotic solvents (dichloromethane (DCM) and acetonitrile (ACN)), presents two emission bands: one at the UV part of the spectrum corresponding to the enol form, and another at the visible region originated by the keto (K) tautomer, while in a nonpolar solvent (n-heptane) only the K emission band is observed.[15] On the other hand, in polar protic media (water or alcohols) where the formation of intermolecular H-bonds is possible, other species as anions, solvated-enols and open-enols can appear.[15] The behavior of HBO can be further complicated by the presence of an electron–donor or –acceptor substituent in the molecular framework.[11, 28-32] These substituent leads to photoinduced intramolecular charge transfer (ICT) reaction at S_1. The ICT and ESIPT events can occur separately or concomitantly.[11, 22, 28-35] Moreover, depending on the substituent character (acceptor or donor) the stepwise proton and charge-transfer reactions might occur in a different order. For example HBO and HBT with electron acceptor substituent (-NO$_2$, -COOH, –COOR or –RCN) lead to an ESIPT reaction followed by an ICT one.[28, 29] However, HBO and HBT having electron donor groups (-NH$_2$, NR$_2$, or –CH$_3$) experience an ICT process prior to the ESIPT one.[11, 30, 31]

Recently, we have studied a HBO derivative containing an electron donor group (-NH$_2$) in the benzoxazole part: 6-amino-2-(2'-hydroxypheny)benzoxazole (6A-HBO).[30, 31] The result of photoexcited 6A-HBO in solution is an ultrafast (80-150 fs) ICT process producing charge-transferred species in which an electron has migrated from the amino-benzoxazole part to the phenol one. This reaction is followed by a slow (up to 100 ps) proton motion leading to a keto tautomer. The dynamics of proton-motion is essentially controlled by the solvent basicity. In solvents like n-heptane and

DCM (*H-bond acceptor ability*, β= 0.0 and 0.1, respectively),[36] an irreversible ESIPT reaction takes place.[31] However, in solvents whose β value is among 0.4-0.55 (ACN, tetrahydrofurane (THF), acetone and dioxane) the proton motion is reversible, thus, the specific interactions between 6A-HBO and solvent molecules play a key role in the nature of the mechanism.[30] Moreover, in polar protic solvents like MeOH, an ESIPT reaction assisted by solvent molecules was observed.[31] HBO in basic, polar and hydroxylic media exhibit an ESPT reaction giving birth to the corresponding anionic species.[15, 18] However, little is known on HBO anion formation and its derivatives in non hydroxylic solvents. To explore the anion formation at both S_0 and S_1 states, we have studied HBO, 6A-HBO and 5-amino-2-(2'-hydroxyphenyl)benzoxazole (5A-HBO) in N,N-dimethylformamide (DMF, β = 0.69).[36]

Here, we report on steady-state and nano- to femtosecond studies of HBO, 6A-HBO, 5A-HBO, and their methoxy derivatives 6-amino-2-(2'-methoxyphenyl)benzoxazole (6A-MBO), and 5-amino-2-(2'-methoxyphenyl)benzoxazole (5A-MBO) in DMF solutions. We found that, the anion of HBO in DMF is generated and stabilized over time at S_0, giving place to a reversible reaction. The emission spectrum of HBO shows the presence of different species (enols, anions and keto ones). Addition of KOH to the DMF solution largely increases the HBO anion population. However, 6A-HBO and 5A-HBO in DMF do not show anion nor keto formation at S_0 and S_1 while open-enol species are formed upon photoexcitation of the closed enol one. Excited 6A-HBO in DMF gives an open enol species due to an ultrafast ICT reaction (80 fs) followed by a solvent relaxation process (2 ps), and slow breaking of the intramolecular H-bond (80 ps). However for 5A-HBO in DMF, a photodegradation was observed, so these ultrafast processes could not be studied. Addition of KOH to the DMF solution leads to the anion formation of the 6A-HBO and 5A-HBO. Our results show how the presence of a substituent in the molecular framework of HBO can largely change the S_0 and S_1 behaviours.

2. Experimental Section

HBO (98 %) was purchased from Sigma-Aldrich and used as received. The synthesis, purification and characterization of 6A-MBO and 6A-HBO are described in our previous report,[31] while those of 5A-MBO and 5A-HBO are described in ESI†.

N,N-dimethylformamide (DMF) (anhydrous, 99,8%) and potassium hydroxide (KOH, 90%) were from Sigma Aldrich and used as received.

The steady-state UV-visible absorption and fluorescence spectra have been recorded using JASCO V-670 and FluoroMax-4 (Jobin-Yvon) spectrophotometers, respectively. Fluorescence quantum yields were measured using Quinine Sulfate in a 0.1 N H_2SO_4 solution as a reference ($\varphi = 0.51$ at 293 K).[37]

Picosecond emission decays were measured using a time-correlated single photon counting (TCSPC) system.[38] For the excitation at 330 nm, we used the second harmonic of the output (660 nm) from a femtosecond optical parametric oscillator (Inspire Auto 100) pumped by 820 nm pulses (90 fs, 250 mW, 80 MHz) from a Ti:sapphire oscillator (Mai Tai HP, Spectra Physics). In this experiment (IRF $\approx$ 30 ps), the femtosecond-laser excitation was set at very low power (<0.5 mW) to avoid undesired photochemistry. For the excitation at 371 and 433 nm, the sample was excited by a 40-ps pulsed diode laser (<5 mW, 40 MHz). The emission signal was collected at the magic angle and the instrument response function (IRF) was ~70 ps. The IRF of the system has been measured using a standard LUDOX (Sigma-Aldrich) solution in 1 cm cell. The decays were deconvoluted and fitted to a single or multiexponential function using the FLUOFIT package (PicoQuant) allowing single and global fits. The quality of the fit was estimated by χ^2, which was always below 1.2, and the distribution of the residues. All experiments were done at 293 K.

The femtosecond (fs) emission transients have been collected using the fluorescence up-conversion technique. The system consists of a femtosecond Ti:sapphire oscillator MaiTai HP (Spectra Physics) coupled to a second harmonic generation and up-conversion setups.[39] The oscillator pulses (90 fs, 250 mW, 80 MHz) were centered at 720 nm and doubled in an optical setup through a 0.5-mm BBO crystal to generate a pumping beam at 360 nm (~ 0.1 nJ/pulse). The polarization of the latter was set to magic angle in respect to the fundamental beam. The sample has been placed in 1-mm thick rotating cell. The fluorescence was focused with reflective optics into a 1-mm BBO crystal and gated with the fundamental fs-beam. The IRF of the full setup (measured as a Raman signal of pure solvent) was ~220 fs. To analyse the decays, a multiexponential function convoluted with the IRF was used to fit the experimental transients. Using this procedure, we can resolve components of ~50 fs. All the experiments were performed at 293 K.

3. Results and Discussion

3.1. Steady-State Absorption Spectra

To begin with, we present and discuss the steady-state behavior of HBO in DMF solution. Figure 1A shows the UV-visible absorption spectra at different gated times after of the sample preparation and at 298 K. The spectra display two low-energy ($\pi\pi^*$) bands centred at 320 and 330 nm, corresponding to the anti- and syn-enol, respectively.[8, 15] Moreover, a new band at 400 nm grows up over time reaching its maximum intensity at t = 335 min (Figure 1A). This band was detected in other basic solvents (MeOH/KOH, EG/KOH, water at pH13) due to the anionic species formed by the deprotonation of the enol ones.[15, 18] The kinetic (inset in Figure 1A) was modelled by a 1:1 reversible scheme using the decrease of absorption intensity of the enol species at 330 nm (ESI†). The direct (k_d) and reverse (k_r) formation rate constants obtained through the model, have values of $3.1 \pm 0.02 \times 10^{-5}$ s^{-1} and $2.2 \pm 0.01 \times 10^{-4}$ s^{-1}, respectively. The small value of k_d is in agreement with the extremely low formation of the anion species in the steady-state absorption spectrum (Figure 1A). The equilibrium constant ($K=k_d/k_r$) is 0.14 ± 0.01 and $\Delta G^o = 4.39 \pm 0.05$ kJ/mol at 298 K. To get ΔH^o and ΔS^o, we have made experiments at different temperatures (from 283 to 323 K) (Figure 1B). The obtained values are $\Delta H^o = 35.58 \pm 0.01$ kJ/mol, $\Delta S^o = 106.1 \pm 0.3$ J/mol.K, indicating that the enthalpy factor is larger than the entropic one. At 298 K, we got $\Delta G^o = 3.96 \pm 0.02$ kJ/mol not very different from the obtained one (4.39 kJ/mol) using the kinetic data. The positive value of ΔH^o indicates that HBO deprotonation process is endothermic, while the change in the standard entropy (ΔS^o) is positive in agreement with a migration of the proton from the dye to DMF molecules. Figure 2 shows the steady-state absorption and emission spectra of HBO (at t = 0 min), 6A-HBO and 5A-HBO together with the corresponding spectra of the methylated molecules (6A-MBO and 5A-MBO) (Scheme 1) in DMF solutions. The absorption spectra of 6A-MBO and 6A-HBO in DMF exhibit a single band whose maximum is at 340 and 350 nm, respectively (Figure 2B). This band without vibrational structure suggests that the $S_0 \rightarrow S_2$ and $S_0 \rightarrow S_1$ transitions are closer than in HBO and 5A-HBO. Compared to HBO absorption (Figure 2A), the shift to longer wavelengths (20 nm, 1730 cm^{-1}) shown by 6A-HBO is due to the effect of the amino group, provoking a large electronic delocalization. When comparing 6A-HBO with 6A-MBO, the bathochromic shift (10

nm, 890 cm^{-1}) is due to the IHB formed in the first one. The band at 350 nm of 6A-HBO is assigned to the enol form as it has a shape similar to that of 6A-MBO. For 5A-MBO and 5A-HBO, $S_0 \rightarrow S_2$ (~275 nm) and $S_0 \rightarrow S_1$ (~320 and ~350 nm) transitions are more separated and show vibrational structures. The $S_0 \rightarrow S_1$ absorption spectra for 5A-MBO and 5A-HBO in DMF present two vibrational bands with their maximum intensities located at 315/345 nm, and 320/350 nm, respectively, (Figure 2C). Here, we also observed a red shift in the 5A-HBO absorption band compared to that of 5A-MBO, due to the effect of the IHB. The amino group in the benzoxazole ring produces a bathochromic shift in the absorption maxima of 6A-HBO and 5A-HBO (350 nm) when compared to that of HBO (330 nm) (Table 1 and 2A). However, 6A-HBO and 5A-HBO show different absorption spectra, reflecting that the position of the amino group involves different changes in the HBO molecular structure. HBO in DMF has a molar extinction coefficient value at 330 nm in DMF of 1.37×10^4 M^{-1} cm^{-1}. The obtained values for 5A-HBO and 6A-HBO at 350 nm in DMF are 0.83×10^4 and 13.4×10^4 M^{-1} cm^{-1}, respectively, showing that the amino group has a positive effect as the oscillator strength of $S_0 \rightarrow S_1$ transition in 6A-HBO.

3.1. Steady-State Fluorescence Spectra

The emission spectrum of HBO in DMF solution exciting at 330 nm (enol absorption region) (Figure 2A) displays a dual emission with maxima located at 360 and 500 nm corresponding to enol and keto forms, respectively (Scheme 1). As a result of the 330 nm excitation, the ESIPT reaction occurs in the syn-enol producing the keto tautomer. Similar behavior has been observed in other basic solvents as MeOH and dimethyl sulfoxide (DMSO).[8, 18] Exciting at 370 nm, HBO exhibits a broad band (full width at half maximum (fwhm) $\approx$ 3120 cm^{-1}) whose intensity maximum is at 450 nm. The Stokes-shift observed here (8080 cm^{-1}) is lower than that obtained when exciting at 330 nm (10300 cm^{-1}, Table 1) leading us to suggest that the ESIPT reaction does not take place when exciting at 370 nm. The emission at 450 nm is due to an anion originated by an ESPT reaction due to the interaction between the dye and DMF molecules (Scheme 1). Studies of HBO in highly basic media (MeOH/KOH, EG/KOH and water pH 13) showed a similar behavior.[12, 16, 33] To further support our assignment, we recorded the fluorescence spectrum of HBO in DMF containing KOH (2 mg of KOH in 5 ml of DMF) upon excitation at 370 nm. Figure S1 (ESI†) shows a

comparison between the emission spectra of HBO in pure DMF and containing KOH. The fluorescence spectrum in pure DMF (exciting at 370 nm) presents the same maximum than that of containing KOH, confirming that the emission is mainly due to the HBO anion. Note that the emission spectrum of HBO in DMF is broader than that in DMF/KOH, suggesting the existence of other species emitting in the blue region and which we assign to the open-enol one. As said above, in pure DMF the anion formation takes place over time, and it is recorded in the absorption spectrum (Figure 1A). Thus, the intermolecular proton transfer occurs both at the S_0 and S_1 states.

The fluorescence spectrum of 6A-HBO in DMF solution exciting at 370 nm is similar to that of its methylated derivative (6A-MBO) being broad (fwhm $\approx$ 3760 cm^{-1}) and with its maximum centred at 450 nm (Figure 2B, Table 2A). Both spectra present an abnormal Stokes-shift (6350 cm^{-1} for 6A-HBO and 7190 cm^{-1} for 6A-MBO), result of an intramolecular charge transfer (ICT) reaction from the amino benzoxazole part to the phenol one, as we reported previously in other media.[30, 31] The high similarity between both emission spectra indicates that for 6A-HBO in DMF there is no evidence of any intramolecular proton transfer, contrary to our previous observations in other solvents where a new red shifted band assigned to the keto form was recorded. [30, 31] The same behavior is observed for 5A-HBO and 5A-MBO where the broad emission band (fwhm $\approx$ 3755 cm^{-1}) has its maximum at 505 nm for both molecules with a Stokes-shift of 8770 and 9180 cm^{-1}, respectively (Figure 2C, Table 2A). As for 6A-HBO, the emission spectrum of 5A-HBO in DMF is practically equal to that of its methylated derivative (5A-MBO). It is clear that no proton transfer takes place within 5A-HBO in DMF. Thus, contrary to the behaviour of HBO in DMF, the emission of 6A-HBO and 5A-HBO are not originated from anion nor keto species. We observed a comparable behaviour for 5A-HBO and 6A-HBO in neutral water solution (pH=7) (Figure S2, ESI†). The presence of the amino group modifies the electronic density of the molecule, precluding then the ESIPT reaction at S_1. DFT calculations show that, the electronic density of HBO at S_0 is mainly localized on the phenol part, while that of 5A-HBO and 6A-HBO is on the benzoxazole one.[32] After a vertical excitation to S_1, the electronic density is redistributed, and it goes in opposite directions for HBO when compared to those of 5A-HBO and 6A-HBO. For the former, it migrates from the phenol part to the benzoxazole one, while for 5A-HBO and 6A-HBO it goes from the amino-benzoxazole moiety to the phenol one. These differences could explain the different behaviors observed for each molecule.[32] The pKa and pKa* for neutral and protonated 5A-HBO

species in water solutions at S_0 and S_1 states (Figures S3 and S4, ESI†) were measured. Those of 6A-HBO and HBO were reported in previous studies (Table 2B).[19, 31, 40] At S_0, the presence of the amino group affects to the electronic density of the imino group (-N=) as it is reflected in the change of its pKa from -0.3[19] for HBO to 3.45[31] and 4.20 for 6A-HBO and 5A-HBO, respectively (Table 2B). However, the electronic density of the OH group is not too much affected at S_0 as its pKa value is similar for the three molecules (10.40[19] for HBO, 10.11[31] for 6A-HBO and 10.15 for 5A-HBO). At S_1, the situation changes, now the pKa* (OH) is different having a value of -0.04[19] or 1.35[40] for HBO, 2.78[31] for 6A-HBO and 5.02 for 5A-HBO (Table 2B). The high value of pKa*(OH) for 6A-HBO and 5A-HBO, shows a decrease in the acidity of this group when compared to HBO. This is probably the reason why in 6A-HBO and 5A-HBO the ESIPT and ESPT reactions do not occur. On the other hand, we obtained the pKa*of the imino group (-N=) being 5.24[19] for HBO, 5.54[31] for 6A-HBO and 7.76 for 5A-HBO (Table 2B). As it is well known, for the IHB formation, a difference of acidity/basicity between the donor and the acceptor group is necessary. At S_0, ΔpKa (pKa (OH-) – pKa (-N=)) is of ~10, 6.66 and 5.95 for HBO, 6A-HBO and 5A-HBO, respectively. However at S_1, ΔpKa* (pKa* (-N=) – pKa* (OH-)) is ~5, 2.76 and 2.74 for HBO, 6A-HBO and 5A-HBO. Thus, we suggest that the small difference in acidity/basicity of 6A-HBO and 5A-HBO at the S_1 state produces the breaking of the IHB when interacting with DMF molecules (H-bond acceptor solvent β = 0.69).[36]

The absorption spectra of HBO, 6A-HBO and 5A-HBO in DMF/KOH exhibit a red-shift band (~ 400 nm) when compared with those obtained in pure DMF (Figure 2), indicating the anions formation at S_0. Figure 3 shows the emission spectra of above molecules in DMF/KOH. The spectra have their maximum intensities similar wavelengths (450 nm), while the one of 5A-HBO has a tail at the red part, which is probably due to the emission of remaining open-ECT forms (Scheme 1). On the other hand, the absorption and emission spectra of 6A-MBO and 5A-MBO in DMF/KOH do not present any change, confirming that there is no anion formation in these solutions (Figures S5 and S6 in ESI†).

The fluorescence excitation spectra are in agreement with the previous discussion. Those of HBO in DMF exhibit three different behaviors following the observation wavelength (Figure 4). At 375 nm observation, only the enol bands (maxima at 320 and 330 nm) are seen. Recording at 425-475 nm, a new band at ~380 nm is detected, in this case the emission mainly corresponds to the anion species.

Recording at 500-600 nm region where the keto form emission is predominant, the absorption band of the syn-enol species is observed. On the other hand, the fluorescence excitation spectra of 6A-HBO and 5A-HBO in DMF together with their methylated derivatives (6A-MBO and 5A-MBO, respectively) display a band similar to that observed in the absorption one, indicating a ground-state common origin of the excited species (Figures S7A-D, ESI†).

The fluorescence excitation spectra are quite different when the DMF solution contains KOH. Now, the fluorescence excitation spectra of HBO and 6A-HBO present a new band around 400 nm which is due to the anion structures. That of 5A-HBO exhibits two different bands, one at 400 nm corresponding to the anion absorption and another one at 350 nm which is the absorption of the remaining open-ECT forms (Figures S8A-D, ESI†) (Scheme 1).

3.3. Picosecond Time-Resolved Fluorescence Study

First, we examine the picosecond photodynamics of HBO in DMF and DMF/KOH solutions exciting at different wavelengths, to get information on the intra- and intermolecular proton transfer reactions. Figure 5 shows representative emission decays of HBO upon excitation at 330, 371 and 433 nm. Table 3 gives the obtained time constants (τ_i), preexponential factors (a_i) and relative contributions (c_i) normalized to 100 after multiexponential global fits. To begin with HBO in DMF solutions, Figure 5A exhibit the gated emission decays exciting at 330 nm and observing at 370 and 550 nm. The decays were well-fitted using a three-exponential function giving time constants of 74 ps, 620 ps and 1.5 ns (Table 3). The 620-ps and 1.5-ns correspond to the main components having contributions (at 370 nm) of 10% and 90%, respectively, and they completely disappear at 450 and 470 nm, respectively. The 74-ps component then appears at 450 nm increasing its relative contribution with the observation wavelength until reaching its maximum (100 %) at the reddest part of the spectrum. Based on previous studies, the 620-ps lifetime is assigned to the open-enol form while that of 1.5-ns is due to the anti-enol one.[8, 15] On the other hand, the 74-ps component is assigned to the emission lifetime of the photoproduced keto form as a result of an ESIPT reaction in the initially excited syn-enol form. The lifetime of the keto specie is comparable to those obtained in other polar and H-bonding acceptor solvents like ACN (80 ps) and

MeOH (60 ps).[15] Figure 5B displays the emission decays of HBO in DMF solution upon excitation at 371 nm and observation at 410 and 550 nm. The fluorescence decays were well-fitted using a biexponential function giving time constants of 620 ps, which has its maximum contribution at the bluest part, and 3.7 ns showing its maximum contribution at the reddest region (Table 3). Based on their contributions at different observation wavelengths, together with the emission spectra (Figure 2A and Figure S1, ESI†), and the previous results when exciting at 330 nm, we suggest that the shortest component (620 ps) is due to the emission of the open-enol species, while the longest one (3.7 ns) is due to the emission of the anion structure. To further support this assignment, we excited at 433 nm (anion absorption band) HBO in pure DMF and containing KOH (Table 3). The obtained emission decays (Figure 5C) were well fitted using a single exponential function giving a time constant of 3.7 ns confirming our previous assignment to the anion emission. Similar values for the emission lifetime of the HBO anion form have been reported in MeOH/KOH (3.1 ns) and ethylene glycol/KOH (3.6 ns).[15]

Now, we discuss the photodynamics of the amino derivatives molecules (6A-HBO, 6A-MBO, 5A-HBO and 5A-MBO). Figures 6 A-B display representative emission decays of 6A-HBO and 5A-HBO in DMF solution upon excitation at 371 nm and recording at different wavelengths. Table 4 gives the obtained τ_i, a_i and c_i from multiexponential global fits for the decays of both molecules and their methylated derivatives. For 6A-HBO in DMF the fit gives a short time constant of 80 ps, which is decaying at 410-450 nm region and rising at 500-550 nm one, and a longer time constant of 1.7 ns. As we explained in the steady-state part, only the emission of open-ECT species is observed. Thus, the 1.7-ns component is assigned to the emission lifetime of this open-ECT, while the shortest component of 80 ps, which is decaying at blue part and rising at red one (Figure S9 in ESI†), is due to the breaking of the IHB between the -OH and the =N- groups (Scheme 2). The emission lifetime of 6A-MBO in DMF, where the proton motion cannot occur, exhibits a monoexponential behavior with a lifetime of 2.6 ns (Table 4) comparable to that of 6A-HBO (1.7 ns), corroborating our assignment of the ns-component to the 6A-HBO open-ECT species. Similar behavior is observed for 5A-HBO in DMF whose fluorescence decays are well fitted by a monoexponential behavior giving a time constant of 7.3 ns (Table 4) corresponding to open-ECT forms, and very similar to that obtained for its methylated derivative 5A-

MBO in DMF (7.9 ns). For 5A-HBO in DMF solution, however, we could not resolve the IHB breaking event, so we conclude that it takes place in less than 10 ps (Scheme 2). For 6A-HBO, the open-ECT lifetime (1.7 ns) is shorter than that of its methylated derivative (2.6 ns) due to an increase in the non-radiative rate constants in the former, most probably enhanced by the IHB breaking and specific interaction with the solvent (Table 2A). For 5A-HBO and 5A-MBO the similar behavior was observed. The quantum yield values (φ) also show that in 6A-HBO (0.4) and 5A-HBO (0.32), unlike 6A-MBO (0.62) and 5A-MBO (0.49), other non-radiative processes are occurring.

Different to HBO, the steady-state emission spectra of these molecules do not show any evidence of the anions formation. We thus studied the ps-photodynamics of 6A-HBO and 5A-HBO in DMF solutions containing KOH. Figure 6C displays the emission decays of 6A-HBO and 5A-HBO in DMF/KOH solution upon excitation at 371 nm and observation at 450 nm. The fluorescence decays of 6A-HBO in DMF/KOH solution exciting at 371 nm are well fitted using a multiexponential function giving the same time constant than those in pure DMF (80 ps and 1.7 ns) in addition to a new one of 3 ns whose maximum contribution is at the red part of the spectrum (Table 5). This new component is also observed when exciting at 433 nm (at this excitation wavelength only the anion specie is excited) (Table 5). Thus, the 3 ns component is due to the emission decay of the anion species formed by an interaction with KOH molecules in DMF solution (Scheme 2). On the other hand, as we described above, the 1.7-ns component (whose maximum contribution is at the blue part) is due to the open-ECT species, while the 80 ps component, which is decaying at the blue part and rising at the red one, reflects the photobreaking of the IHB and formation of the intermolecular one. 5A-HBO in DMF/KOH solution show a similar behavior when exciting at 371 nm, giving two lifetimes of 3.2 and 7.3 ns (Table 5). The 3.2 ns component, which is observed when the excitation is 433 nm (Table 5), is assigned to the emission of the anion species, while the 7.3 ns component is due to the emission of the open-ECT one (Scheme 2). For 5A-HBO in pure DMF, we cannot observe the breaking of the IHB and we suggest that it takes place in less than 10 ps (Scheme 2).

3.3. Femtosecond Dynamics

To investigate the ultrafast dynamics, we carried out up-conversion fs-emission experiments using the above solutions. We found, a photodegradation of HBO, 5A-HBO and 5A-MBO in DMF solutions, making not possible their photodynamics study. For HBO, upon fs-pulse irradiation, we observed the formation of the phenolate-type anion species, as the recorded absorption and emission spectra are comparable to those obtained for HBO in DMF/KOH (Figure S10, ESI† and Figure S3, respectively). However, for 5A-HBO we observed a large decrease in the emission intensity and a big change in the absorption spectrum, showing a blue-shift in the maximum and a long red-shifted tail (Figure S11, ESI†). Based on the strongly quenched emission and the long absorption tail, the photoproduct of irradiated 5A-HBO could not be of anions nature. The anions strongly emit and have well defined absorption band (Figure 3). The photodegradation of 5A-MBO in DMF suggests that the OH group of the 5A-HBO may not be involved in its photodegradation. However, 6A-MBO and 6A-HBO solutions were photostable to record the fs-dynamics. We excited at 360 nm where the molecular system is brought to the S_1 state without excess of vibrational energy. Figure 7 presents the obtained fluorescence transients at different regions of the emission spectra. Table 6 gives the obtained time constants and preexponential factors from a multiexponential fit taking into account the values obtained from the ps-ns experiments.

The ultrafast dynamics of 6A-MBO in DMF solutions was examined, and here only the ICT reaction is expected (Figure 7A). The longest component (2.3 ns) is fixed in the fit. At the bluest part of the emission spectrum (380-420 nm), an ultrafast rising component (~80 fs) together with a fast decaying one (1.8-2 ps) are observed (Table 6). On the other hand, at the reddest region (450-550 nm) the fs-component is not present and the 1.8-2 ps one appears now as a rising signal. Based on previous studies,[30, 31] we assign the 80-fs component to an ultrafast ICT reaction from the aniline group to the MBO molecular frame (Scheme 3A), together with the ultrafast inertial solvent response which happen in less than 100 fs.[41] The ~2 ps component is assigned to solvent relaxation as well as VR/cooling processes happening in this time regime. This component is similar to that obtained for coumarin 153 in DMF assigned to solvent relaxation (2 ps).[41]

The ultrafast dynamics of 6A-HBO in DMF solution was investigated. The results show a comparable behavior to that of 6A-MBO (Figure 7B and Table 6). This is in agreement with what we observed in the emission spectra. Thus, as for 6A-MBO, at the bluest part of the emission spectrum (380-420 nm), an ultrafast rising component of ~80 fs with a fast decaying one of 1.8-2 ps are observed, while at the reddest region only the ps-component appears as a rise. The 80-fs is attributed to the ICT reaction and the 1.8-2 ps one is due to solvent relaxation together with VR/cooling processes as stated earlier (Scheme 3B). From these results, we suggest that 6A-MBO and 6A-HBO in DMF solutions exhibit the same ultrafast ICT reaction and the IHB in the latter does not play much role in the related dynamics. Subsequent to these events, 6A-HBO shows the breaking of the IHB giving open-ECT from syn-enol forms in 80 ps. The proton motion here is governed by the ICT reaction and the interactions with the DMF molecules.

We could not carry out fs-studies of the anion species of HBO, 6A-HBO and 5A-HBO in DMF/KOH solutions, due to the high instability of the samples upon femtosecond laser excitation.

4.   Conclusions

In this work, we have reported on studies of the steady-state and the photodynamical behaviors of HBO and its amino derivatives, 6A-HBO and 5A-HBO, in DMF and DMF/KOH solutions. At S_0 state, HBO in DMF solution presents a reversible deprotonation/protonation where the anion is generated (K = 0.14 and ΔG^o = 4.4 kJ/mol, at 298 K). Moreover, at S_1 state, HBO exhibits an ESIPT reaction to give the keto tautomer. Exciting at different regions, we observed different emitting species: open-enol (620 ps), anti-enol (1.5 ns), keto (74 ps) and anion (3.7 ns). However, 6A-HBO and 5A-HBO do not show any proton transfer reaction but display a unique broad emission band (similar to its methylated derivatives 6A-MBO and 5A-MBO, respectively) with a lifetime of 1.7 ns (2.6 for 6A-MBO), and 7.3 ns (7.9 ns for 5A-MBO), respectively. These formed species are assigned to open-ECT structures. Femtosecond studies of 6A-HBO and 6A-MBO in DMF solutions shows an ultrafast ICT reaction (80 fs) followed by a solvent relaxation process (2 ps). Subsequently, a breaking of the IHB and formation of the intermolecular one for 6A-HBO (in 80 ps) and 5A-HBO (in <10 ps) take place. The emission lifetimes of 6A-HBO and 5A-HBO anion formed in DMF/KOH are 3.0 and 3.2 ns, respectively. The presence and position of the amino group in HBO modify the photodynamics behaviour of the related compound.

Our results show how intramolecular H-bond is sensitive to the environment producing intermolecular interactions.

Acknowledgments

Electronic Supplementary Information (ESI†) Available: Reversible model explanation and thermodynamic constants calculation (ΔH^o, ΔS^o and ΔG^o), Figure S1 shows the emission fluorescence spectra of HBO in DMF and DMF/KOH solutions, Figure S2 is the emission spectra of 6A-MBO, 6A-HBO, 5A-MBO, and 5A-HBO in neutral water solution, Figures S3 and S4 present UV-visible absorption and emission spectra of 5A-HBO in different pH solutions, Figure S5 and S6 display the UV-visible absorption and fluorescence spectra of 6A-MBO and 5A-MBO in DMF and DMF/KOH solutions, respectively, Figures S7 and S8 show the excitation fluorescence and absorption spectra of HBO, 6A-HBO, 6A-MBO, 5A-HBO and 5A-MBO in DMF and DMF/KOH solutions, respectively, Figure S9 presents the magic-angle emission decay of 6A-HBO in DMF solution, Figures S10 and S11 show UV-visible absorption and fluorescence spectra of HBO and 5A-HBO in DMF solution upon fs-pulse irradiation. Figures S12-S17 giving the ^{1}H (A) and ^{13}C (B) NMR spectra of different molecules in DMSO-d_6. See DOI:

References

1. G. J. Woolfe, M. Melzig, S. Schneider and F. Dörr, *Chem. Phys.*, 1983, **77**, 213-221.
2. C. A. S. Potter and R. G. Brown, *Chem. Phys. Lett.*, 1988, **153**, 7-12.
3. K. Das, N. Sarkar, D. Majumdar and K. Bhattacharyya, *Chem. Phys. Lett.*, 1992, **198**, 443-448.
4. A. Douhal, F. Amat-Guerri, M. P. Lillo and A. U. Acuna, *J. Photochem. and Photobiol. A: Chemistry*, 1994, **78**, 127-138.
5. M. A. Rios and M. C. Rios, *J. Phys. Chem.*, 1995, **99**, 12456-12460.
6. D. P. Zhong, A. Douhal and A. H. Zewail, *Proc. Natl. Acad. Sci. U.S.A.*, 2000, **97**, 14056-14061.
7. P. Purkayastha and N. Chattopadhyay, *Phys. Chem. Chem. Phys.*, 2000, **2**, 203-210.
8. O. K. Abou-Zied, R. Jimenez, E. H. Z. Thompson, D. P. Millar and F. E. Romesberg, *J. Phys. Chem. A*, 2002, **106**, 3665-3672.
9. H. Wang, H. Zhang, O. K. Abou-Zied, C. Yu, F. E. Romesberg and M. Glasbeek, *Chem. Phys. Lett.*, 2003, **367**, 599-608.
10. M. Rini, J. Dreyer, E. T. J. Nibbering and T. Elsaesser, *Chem. Phys. Lett.*, 2003, **374**, 13-19.
11. Y.-M. Cheng, S.-C. Pu, C.-J. Hsu, C.-H. Lai and P.-T. Chou, *ChemPhysChem*, 2006, **7**, 1372-1381.
12. O. F. Mohammed, S. Luber, V. S. Batista and E. T. J. Nibbering, *J. Phys. Chem. A*, 2011, **115**, 7550-7558.

13. O. K. Abou-Zied, *Phys. Chem. Chem. Phys.*, 2012, **14**, 2832-2839.
14. Y. Houari, S. Chibani, D. Jacquemin and A. D. Laurent, *J. Phys. Chem. B*, 2014.
15. N. Alarcos, B. Cohen and A. Douhal, *J. Phys. Chem. C*, 2014, **118**, 19431-19443.
16. P. Wnuk, G. Burdzinski, M. Sliwa, M. Kijak, A. Grabowska, J. Sepiol and J. Kubicki, *Phys. Chem. Chem. Phys.*, 2014, **16**, 2542-2552.
17. G. Zhang, H. Wang, Y. Yu, F. Xiong, G. Tang and W. Chen, *Appl. Phys. B*, 2003, **76**, 677-681.
18. O. K. Abou-Zied, *Chem. Phys.*, 2007, **337**, 1-10.
19. M. Krishnamurthy and S. K. Dogra, *J. Photochem.*, 1986, **32**, 235-242.
20. R. S. Becker, C. Lenoble and A. Zein, *J. Phys. Chem.*, 1987, **91**, 3509-3517.
21. T. Elsaesser and B. Schmetzer, *Chem. Phys. Lett.*, 1987, **140**, 293-299.
22. W. Frey, F. Laermer and T. Elsaesser, *J. Phys. Chem.*, 1991, **95**, 10391-10395.
23. S. Lochbrunner, A. J. Wurzer and E. Riedle, *J. Phys. Chem. A*, 2003, **107**, 10580-10590.
24. S. M. Aly, A. Usman, M. AlZayer, G. A. Hamdi, E. Alarousu and O. F. Mohammed, *J. Phys. Chem. B*, 2014.
25. H. K. Sinha and S. K. Dogra, *Chem. Phys.*, 1986, **102**, 337-347.
26. T. Elsaesser and W. Kaiser, *Chem. Phys. Lett.*, 1986, **128**, 231-237.
27. A. P. Fluegge, F. Waiblinger, M. Stein, J. Keck, H. E. A. Kramer, P. Fischer, M. G. Wood, A. D. DeBellis, R. Ravichandran and D. Leppard, *J. Phys. Chem. A*, 2007, **111**, 9733-9744.
28. C. H. Kim, J. Park, J. Seo, S. Y. Park and T. Joo, *J. Phys. Chem. A*, 2010, **114**, 5618-5629.
29. C.-C. Hsieh, Y.-M. Cheng, C.-J. Hsu, K.-Y. Chen and P.-T. Chou, *J. Phys. Chem. A*, 2008, **112**, 8323-8332.
30. M. Gutierrez, N. Alarcos, M. Liras, F. Sánchez and A. Douhal, *J. Phys. Chem. B*, 2015, **119**, 552-562.
31. N. Alarcos, M. Gutiérrez, M. Liras, F. Sánchez and A. Douhal, *Phys. Chem. Chem. Phys. DOI: 10.1039/C5CP00577A*, 2015.
32. N. Alarcos, M. Gutiérrez, M. Liras, F. Sánchez, M. Moreno and A. Douhal, *Phys Chem Chem Phys*, 2015, **Submitted**.
33. A. Douhal, M. Sanz, M. A. Carranza, J. A. Organero and L. Santos, *Chem. Phys. Lett.*, 2004, **394**, 54-60.
34. A. D. Roshal, J. A. Organero and A. Douhal, *Chem. Phys. Lett.*, 2003, **379**, 53-59.
35. J. Seo, S. Kim and S. Y. Park, *J. Am. Chem. Soc.*, 2004, **126**, 11154-11155.
36. M. J. Kamlet, J. L. M. Abboud, M. H. Abraham and R. W. Taft, *J. Org. Chem.*, 1983, **48**, 2877-2887.
37. R. A. Velapoldi and K. D. Mielenz, *Appl. Opt.*, 1981, **20**, 1718-1718.
38. J. A. Organero, L. Tormo and A. Douhal, *Chem. Phys. Lett.*, 2002, **363**, 409-414.
39. M. Gil and A. Douhal, *Chem. Phys. Lett.*, 2006, **428**, 174-177.
40. E. L. Roberts, J. Dey and I. M. Warner, *J. Phys. Chem.*, 1996, **100**, 19681-19686.
41. M. L. Horng, J. A. Gardecki, A. Papazyan and M. Maroncelli, *J. Phys. Chem.*, 1995, **99**, 17311-17337.

Caption of figures, schemes and tables.

Scheme 1. Possible molecular structures of HBO, 6A-MBO, 6A-HBO, 5A-MBO and 5A-HBO.

Scheme 2. Proposed photodynamics mechanism of 6A-HBO and 5A-HBO at picosecond-nanosecond scale in DMF solutions and adding KOH.

Scheme 3. Proposed photodynamics mechanisms of (A) 6A-MBO and (B) 6A-HBO at femtosecond-picosecond scale in DMF solution. The arrows indicate the nature of the photoreaction in the related structure. See text for detail.

Table 1. Values of the spectroscopic and photo physical parameters of HBO in DMF solutions determined in this work.

Table 2. Values of the spectroscopic and photo physical parameters of (A) 6A-MBO, 6A-HBO, 5A-MBO and 5A-HBO in DMF solutions determined in this work. (B) pKa values of the –N= of the benzoxazole ring and of the OH- of the phenyl one, in the steady and excited state of HBO, 6A-HBO and 5A-HBO obtained in this work and in previous studies.

Table 3. Values of the time constants (τ_i), normalized (to 100) pre-exponential factors (a_i) and fractional contributions ($c_i = \tau_i a_i$) obtained from a multiexponential fit of the emission picosecond-nanosecond decays of the HBO upon excitation at 330, 371 and 433 nm in DMF and DMF/KOH (only exciting at 433 nm) solutions, at the observation wavelength as indicated. A negative sign of a_i (c_i) indicates a rising component in the emission signal.

Table 4. Values of the time constants (τ_i), normalized (to 100) pre-exponential factors (a_i) and fractional contributions ($c_i = \tau_i a_i$) obtained from a fit of the emission picosecond-nanosecond decays of 6A-HBO, 6A-MBO, 5A-HBO and 5A-MBO in DMF solution, upon excitation at 371 nm, and at the observation wavelength as indicated. A negative sign of a_i (c_i) indicates a rising component in the emission signal.

Table 5. Values of the time constants (τ_i), normalized (to 100) pre-exponential factors (a_i) and fractional contributions ($c_i = \tau_i a_i$) obtained from a fit of the emission picosecond-nanosecond decays of 6A-HBO and 5A-HBO in DMF/KOH solution, upon excitation at 371 and 433 nm, and at the observation wavelength as indicated. A negative sign of a_i (c_i) indicates a rising component in the emission signal.

Table 6. Values of the time constants (τ_i), normalized (to 100) pre-exponential factors (a_i) of the functions used in fitting the femtosecond-emission transients of 6A-MBO and 6A-HBO in DMF solution, upon excitation at 350 nm and observation as indicated. A negative sign of a_i (c_i) indicates a rising component in the emission signal.

Figure 1. (A) Variation of UV-visible absorption spectrum of HBO in a DMF solution over time (0, 10, 20, 30, 40, 50, 60, 70, 90, 115, 135, 160, 185, 215, 275, 335 min). The inset shows the kinetic representation for a reversible model 1:1. The solid line is the best fit assuming this model. (B) Variation of UV-visible absorption spectrum of HBO in a DMF solution (equilibrated system) with the temperature (10, 15, 20, 25, 30, 35, 37.5, 40, 45 and 50 ºC).

Figure 2. Normalized UV-visible absorption and fluorescence spectra (upon excitation at 330 (only for HBO) and at 370 nm) of (A) HBO, (B) 6A-HBO (red solid line) and 6A-MBO (blue dashed line), and (C) 5A-HBO (green solid line) and 5A-MBO (pink dotted line) in DMF solution.

Figure 3. Normalized UV-visible absorption and fluorescence spectra (upon excitation at 370 nm) of HBO (black solid line), 6A-HBO (blue dashed line) and 5A-HBO (red dotted line) in DMF/KOH solution.

Figure 4. Excitation fluorescence and absorption spectra of HBO in DMF solution. The observation wavelengths are shown in the inset.

Figure 5. Magic-angle emission decays of HBO in DMF solution exciting (A) at 330 and (B) at 370 nm, and observing at the wavelengths indicated in the inset. (C) Magic-angle emission decays of HBO in (1) DMF and (2) DMF/KOH solution exciting at 433 nm and observing at 450 nm. The solid lines are from the best-fit using multiexponential functions and the IRF is the instrumental response function.

Figure 6. Magic-angle emission decays of 6A-HBO and 5A-HBO in DMF solution exciting at 371 nm and observing at (A) 450 nm and (B) 500 nm. (C) Magic-angle emission decays of same molecules DMF/KOH solution exciting at 371 nm and observing at 450 nm. The solid lines are from the best-fit using multiexponential functions and the IRF is the instrumental response function.

Figure 7. Representative magic-angle femtosecond-emission transients of (A) 6A-MBO and (B) 6A-HBO in a DMF solution. The samples were excited at 350 nm and recorded at the indicated wavelengths. The solid lines are from the best multiexponential fits, and the IRF (dashed line) is the instrumental response function.

Scheme 1.
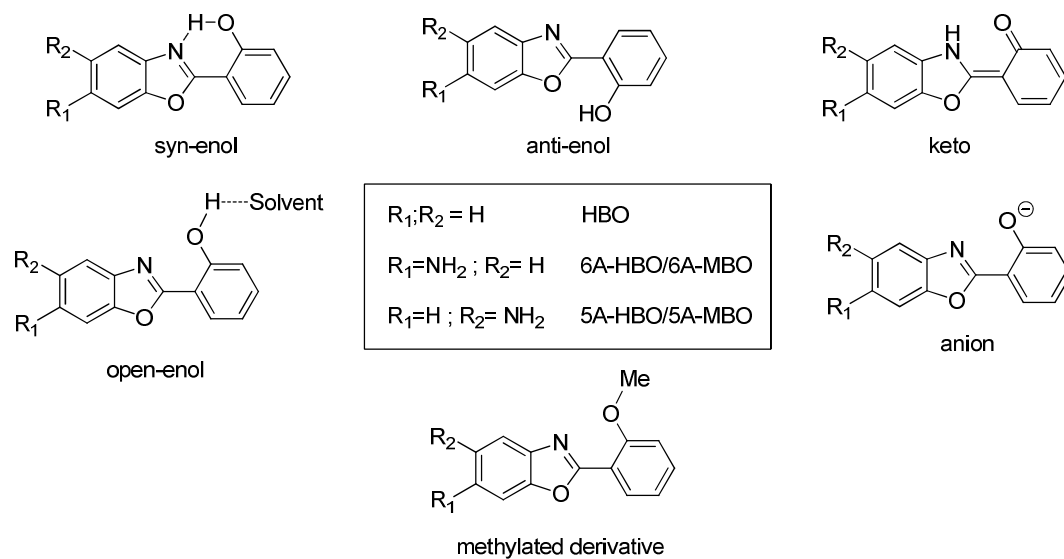
Scheme 2.
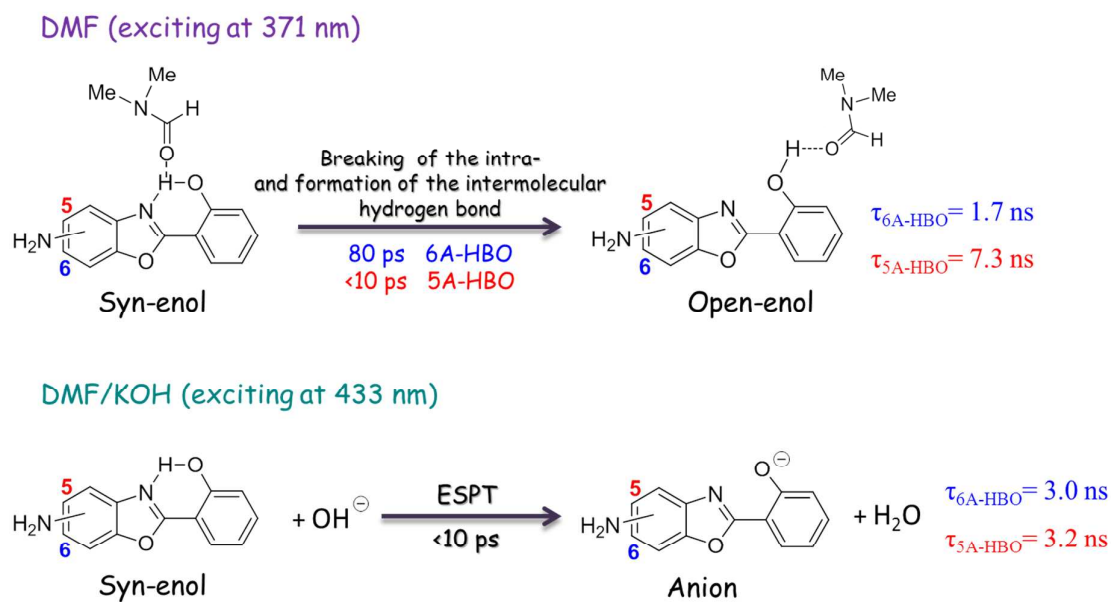
Scheme3.
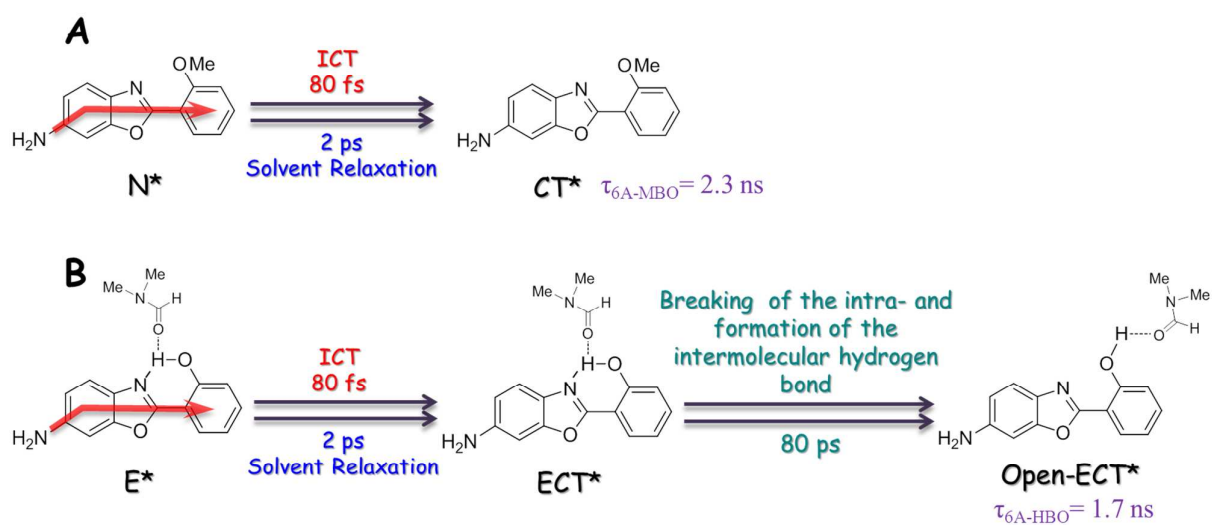
Figure 1.
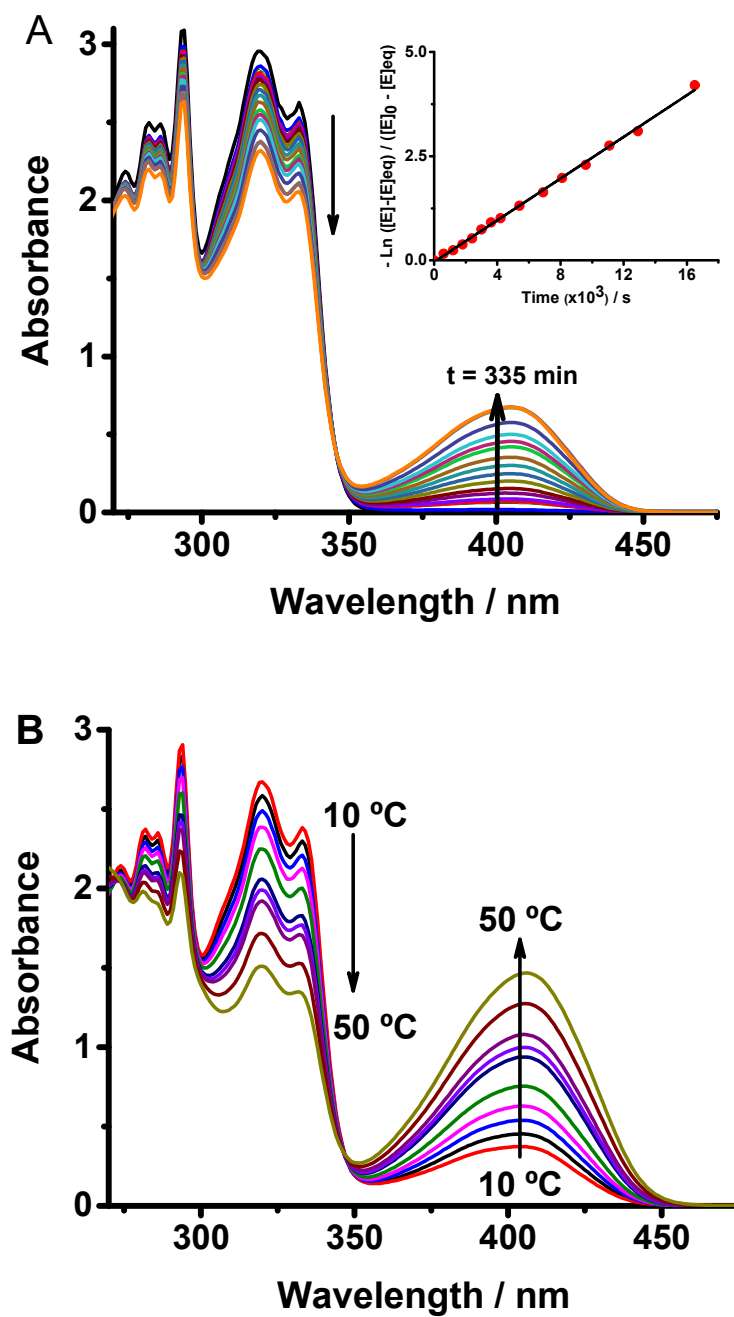
Figure 2.
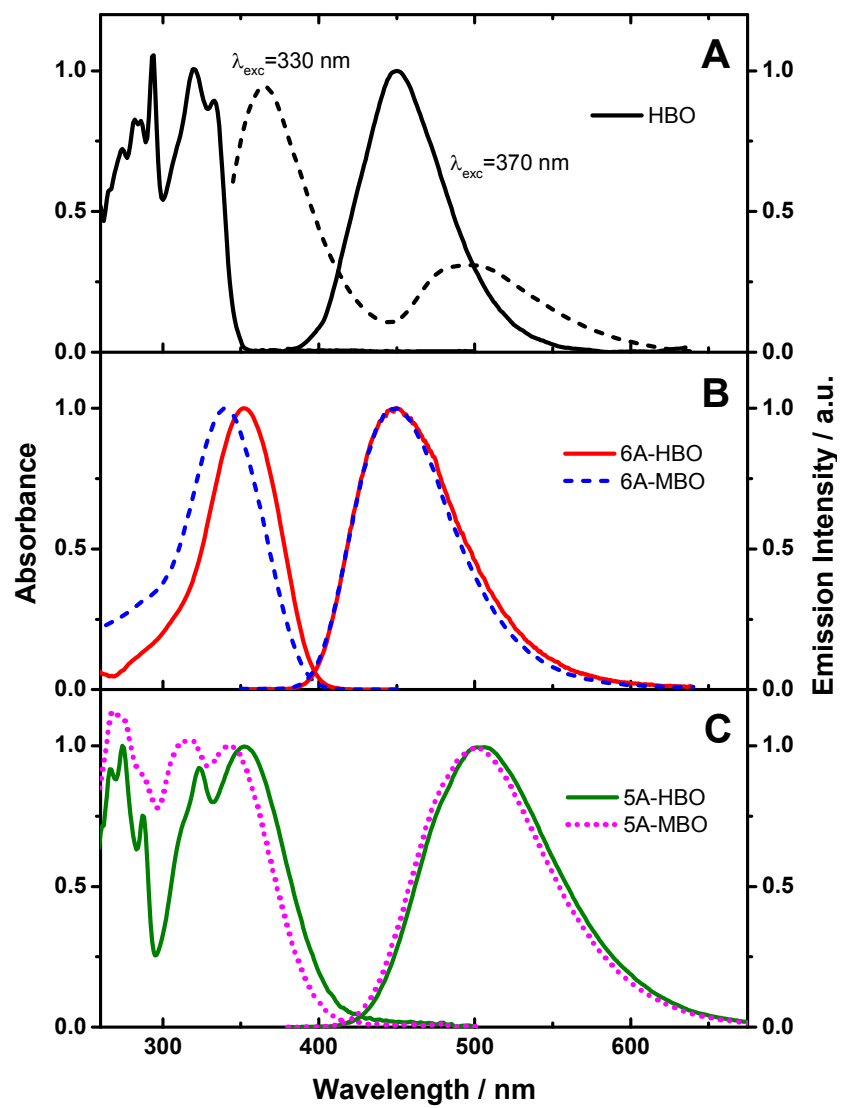
Figure 3.
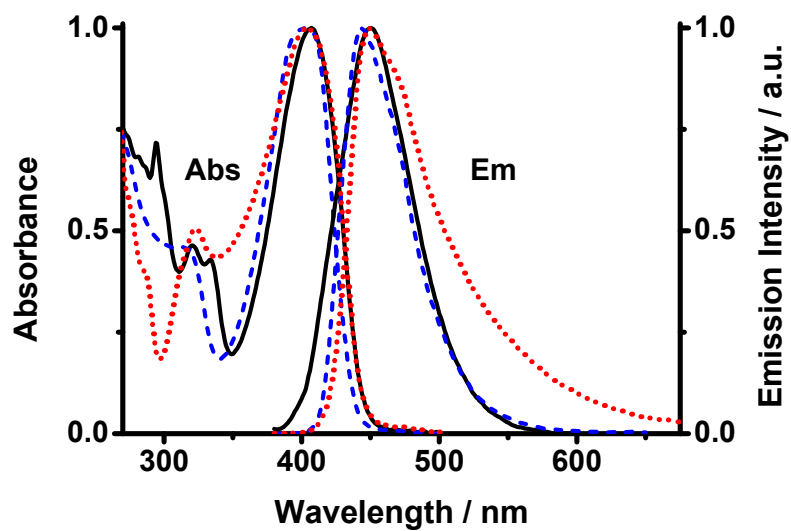
Figure 4.
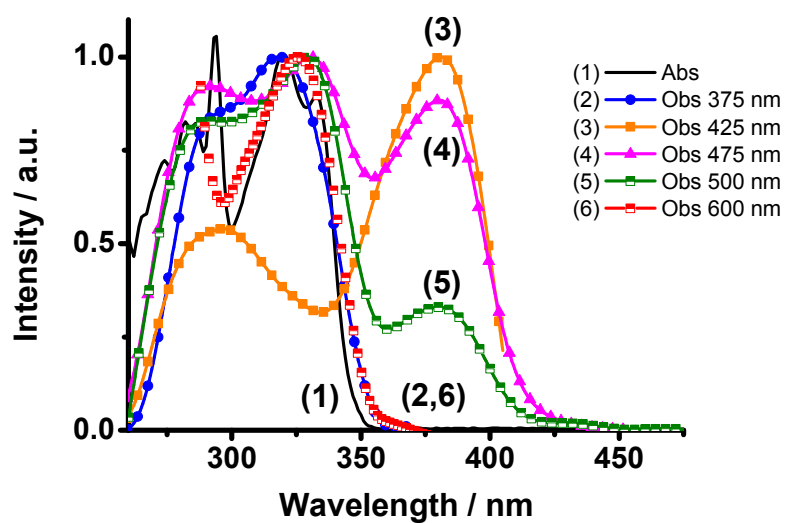
Figure 5.
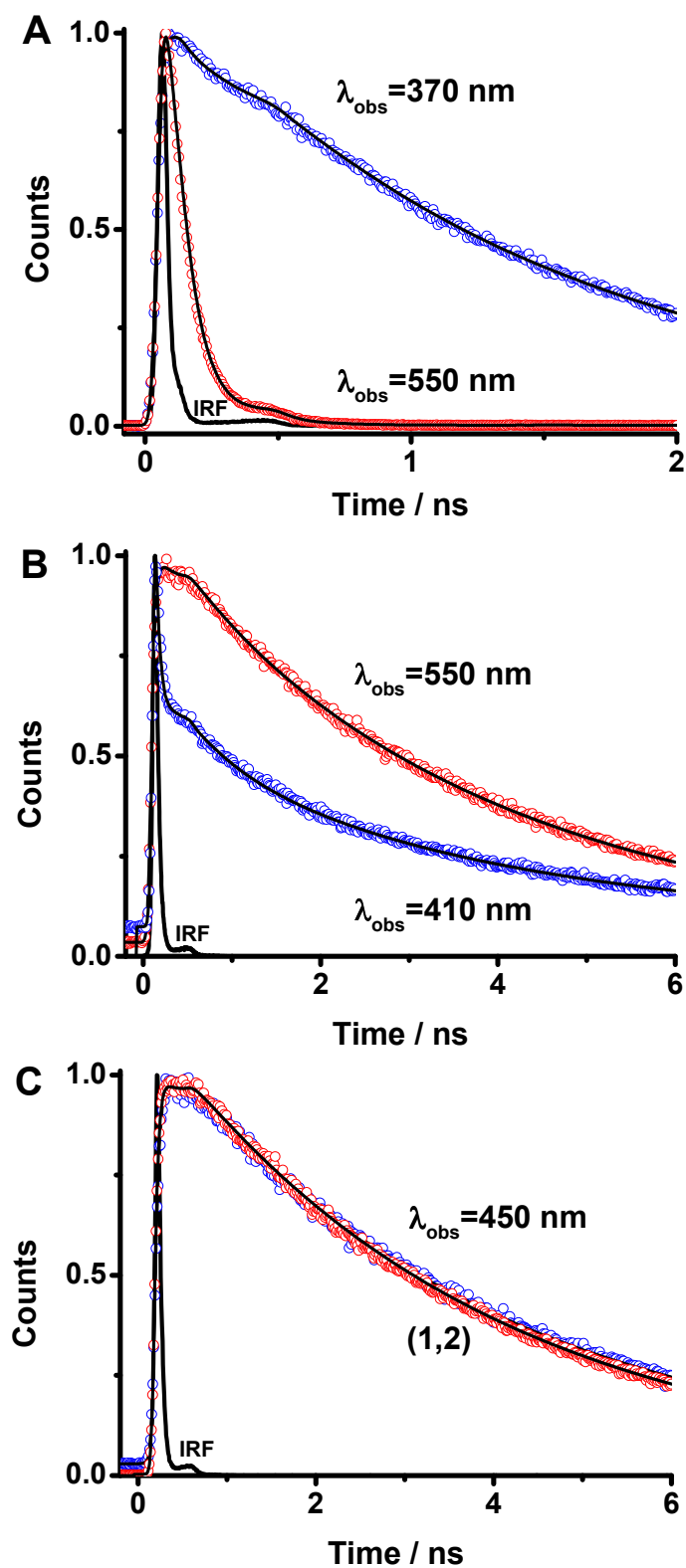
Figure 6.
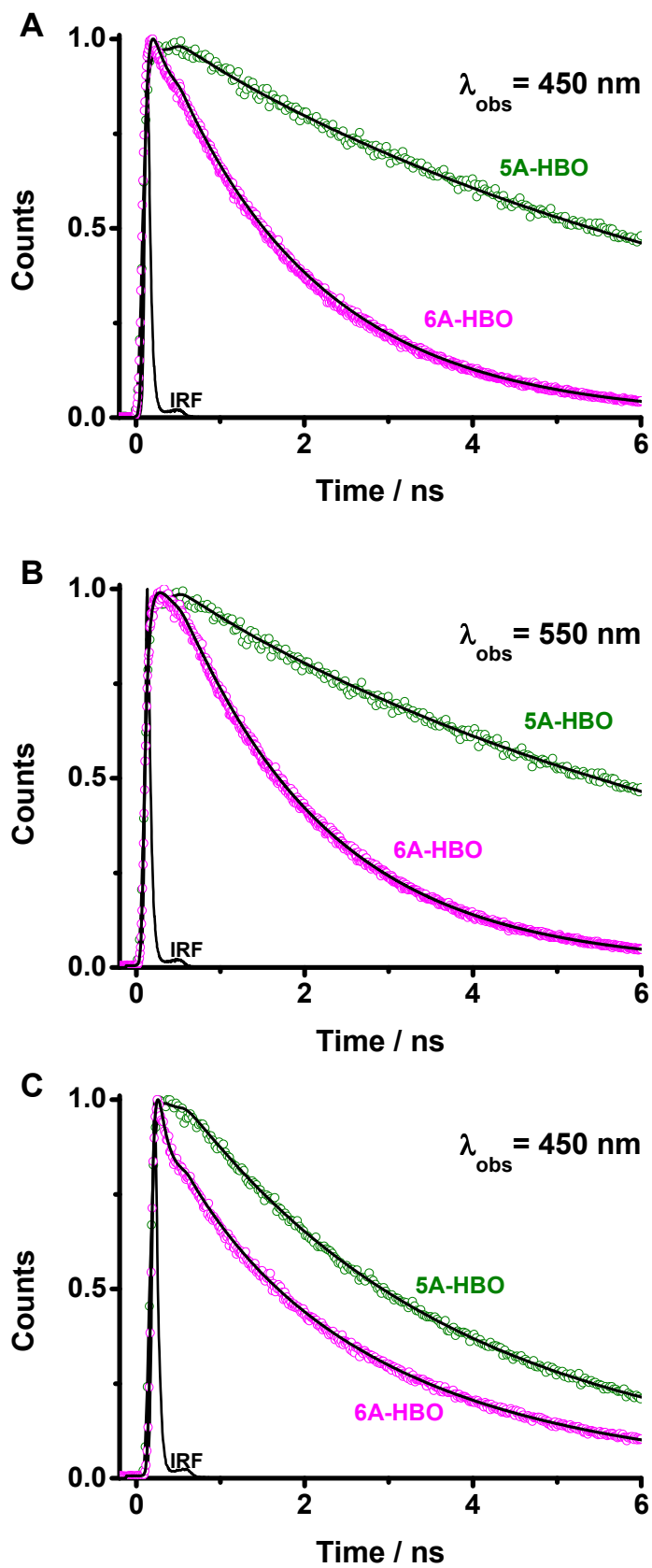
Figure 7.
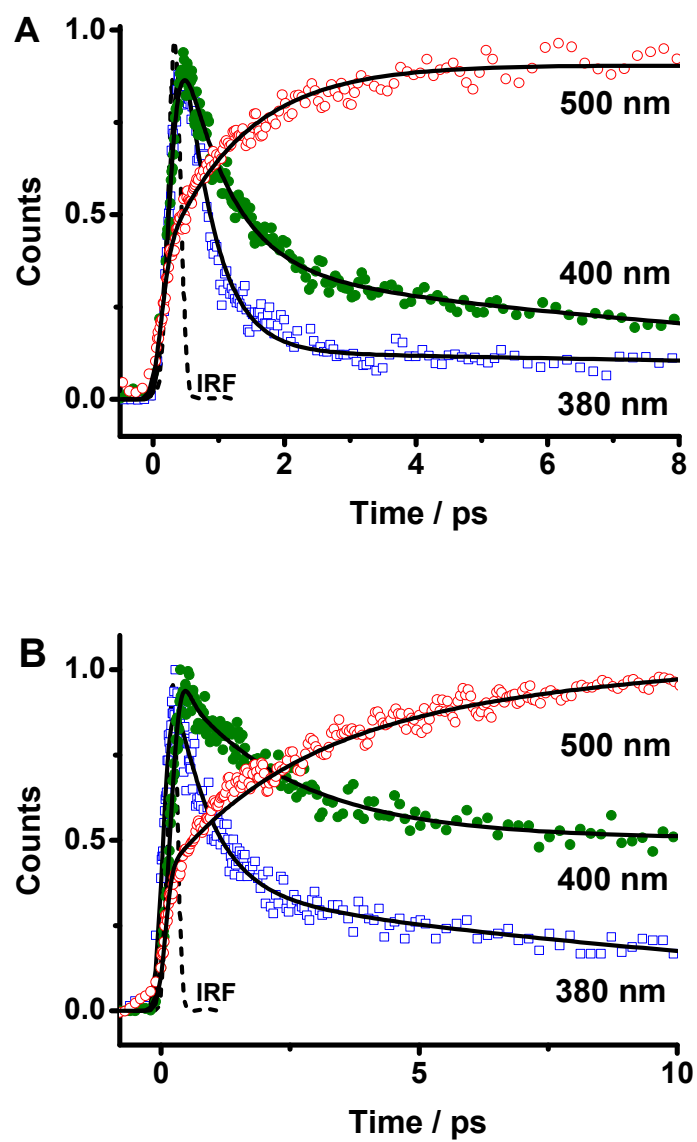
Table 1.

	HBO
λ_{abs} **(E)/ nm**	320-330
λ_{em} **(E*, K*) / nm**	360, 500
$\Delta\nu_{ss}$ **(E*, K*)/ cm^{-1}**	2525, 10300
fwhm (E*, K*)/ cm^{-1}	4150, 3195
τ **(E*) / ns**	0.62 ± 0.05,
	1.5 ± 0.2
τ **(K*) / ps**	74 ± 2
φ **(E*)^a**	0.01 ± 0.001
φ **(K*)**	0.003 ± 1x10^4
k_r **(E*) / 10^8 s^{-1}**	0.1 ± 0.02
k_{nr} **(E*) / 10^8 s^{-1}**	9.3 ± 0.1
k_r **(K*) / 10^8 s^{-1}**	0.4 ± 0.03
k_{nr} **(K*) / 10^8 s^{-1}**	135 ± 0.9

Table 2. ^{a}Calculated from the average of the enol lifetimes

A)	6A-MBO	6A-HBO	5A-MBO	5A-HBO
λ_{abs} **/ nm**	340	350	345	350
λ_{em} **(CT) / nm**	450	450	505	505
$\Delta\nu_{ss}$ **/ cm^{-1}**	7190	6350	9180	8770
fwhm / cm^{-1}	3760	3760	3755	3755
τ **(± 0.1) (CT) / ns**	2.3	1.7	7.9	7.3
φ **(± 0.02)**	0.62	0.4	0.49	0.32
k_r **/ 10^8 s^{-1}**	2.4 ± 0.1	2.3 ± 0.1	0.52 ± 0.01	0.54 ± 0.02
k_{nr} **/ 10^8 s^{-1}**	1.5 ± 0.1	3.5 ± 0.1	0.65 ± 0.03	0.93 ± 0.03

B)	pKa(-N=)	pKa*(-N=)	pKa(OH-)	pKa*(OH-)
HBO	-0.30±0.02^a	5.24±0.1^a	10.40±0.12^a	-0.04±0.02^a/ 1.35±0.05^b
6A-HBO	3.45±0.12^c	5.54±0.09^c	10.11±0.15^c	2.78±0.11^c
5A-HBO	4.20±0.2	7.76±0.1	10.15±0.13	5.02±0.1

Table 3.

λ_{exc} / nm	λ_{Obs}	τ_1 / ps (± 2)	$a_1\%$	$c_1\%$	τ_2 / ps (± 5)	$a_2\%$	$c_2\%$	τ_3 / ns (± 0.2)	$a_3\%$	$c_3\%$
330	370	-	-	-	620	10	5	1.5	90	95
	450	74	89	28	620	2	4	1.5	9	68
	470	74	99	84	-	-	-	1.5	1	16
	575	74	100	100	-	-	-	-	-	-

λ_{exc} / nm	λ_{Obs}	τ_1 / ps (± 10)	$a_1\%$	$c_1\%$	τ_2 / ps (± 0.4)	$a_2\%$	$c_2\%$
371	410	620	30	4	3.7	70	96
	450	620	12	2	3.7	88	98
	475	620	9	2	3.7	91	98
	550	-	-	4	3.7	100	100

λ_{exc} / nm	λ_{Obs}	τ_1 / ps (± 0.4)	$a_1\%$	$c_1\%$
433	410	3.7	100	100
	450	3.7	100	100
	475	3.7	100	100
	500	3.7	100	100
433 **With KOH**	450	3.7	100	100
	475	3.7	100	100
	500	3.7	100	100
	550	3.7	100	100

Table 4.

Dye	λ_{Obs}	τ_1 / ps (± 2)	$a_1\%$	$c_1\%$	τ_2 / ns (± 0.2)	$a_2\%$	$c_2\%$
6A-HBO	410	80	23	2	1.7	77	98
	450	80	20	1	1.7	80	99
	500	80	(-)100	(-)100	1.7	100	100
	550	80	(-)100	(-)100	1.7	100	100

	λ_{Obs}	τ_1 / ps (± 0.4)	$a_1\%$	$c_1\%$
6A-MBO	410	2.6	100	100
	450	2.6	100	100
	500	2.6	100	100
	550	2.6	100	100
5A-HBO	410	7.3	100	100
	450	7.3	100	100
	500	7.3	100	100
	600	7.3	100	100
5A-MBO	410	7.9	100	100
	450	7.9	100	100
	500	7.9	100	100
	600	7.9	100	100

Table 5.

Dye (λ_{exc}/nm)	λ_{Obs}	τ_1 / ps (± 2)	a_1%	c_1%	τ_2 / ns (± 0.2)	a_2%	c_2%	τ_3 / ns (± 0.3)	a_3%	c_3%
6A-HBO (371)	410	80	12	2	1.7	35	30	3.0	53	68
	450	80	8	1	1.7	15	10	3.0	77	89
	500	80	(-)100	(-)100	1.7	11	6	3.0	89	94
	550	80	(-)100	(-)100	1.7	8	7	3.0	92	95

	λ_{Obs}	τ_1 / ps (± 0.3)	a_1%	c_1%	τ_2 / ps (± 0.5)	a_2%	c_2%
5A-HBO (371)	410	3.2	92	85	7.3	8	15
	450	3.2	88	76	7.3	12	24
	475	3.2	77	60	7.3	23	40
	550	3.2	19	10	7.3	81	90

	λ_{Obs}	τ_1 / ps (± 0.3)	a_1%	c_1%
6A-HBO (433)	450	3.0	100	100
	475	3.0	100	100
	500	3.0	100	100
	550	3.0	100	100
5A-HBO (433)	450	3.2	100	100
	475	3.2	100	100
	500	3.2	100	100
	550	3.2	100	100

Table 6.

Dye	λ_{Obs} / nm	τ_1 / fs (± 2)	$a_1\%$	τ_2 / ps (± 0.2)	$a_2\%$	τ_3 / ps (± 1)	$a_3\%$	τ_4^* / ns (± 0.1)	$a_4\%$
6A-MBO	380	80	-100	1.8	92	-	-	2.3	8
	400	80	-100	1.8	69	-	-	2.3	31
	420	80	-100	1.8	34	-	-	2.3	66
	450	-	-	1.8	-100	-	-	2.3	100
	475	-	-	1.8	-100	-	-	2.3	100
	500	-	-	2.0	-100	-	-	2.3	100
	550	-	-	2.0	-100	-	-	2.3	100
6A-HBO	380	80	-100	1.8	82	80	15	1.7	3
	400	80	-100	1.8	38	80	32	1.7	30
	420	80	-100	1.8	19	80	38	1.7	45
	450	-	-	1.8	-100	80	41	1.7	59
	475	-	-	1.8	-100	80	52	1.7	48
	500	-	-	2.0	-75	80	-25	1.7	100
	550	-	-	2.0	-44	80	-56	1.7	100

Figure for the TOC:

Proposed photodynamics mechanisms of 6A-HBO at femtosecond-picosecond scale in DMF solution.

6A-HBO